Design of Aircraft On-Glass Antennas Using a Coupled Feed Structure

Gangil Byun, Chulhun Seo, Byung-Jun Jang, and Hosung Choo

***Abstract*—This communication proposes a glass-integrated antenna using a coupled feed structure for military FM radio communications on aircraft. The proposed antenna consists of a feed strip and two radiators, printed on the left-side window of the cockpit. The proposed antenna structure is optimized with the genetic algorithm in conjunction with the FEKO EM simulator. The optimized antenna is built and installed on a 1/10-sized KUH-Surion mock-up and antenna performance, such as reflection coefficient and bore-sight gain, is measured in a semi-anechoic chamber. The optimized antenna shows a half-power matching bandwidth of 28% at the center frequency of the military FM radio band and an average bore-sight gain of about -2.60 dBi. The results show that the proposed antenna is suitable for use as a military FM antenna for aircraft applications.**

***Index Terms*—Aircraft antenna, coupled feed structure, FM antenna, glass-integrated antenna.**

I. Introduction

Military FM radio (30 MHz–88 MHz) is generally used for aircraft voice or data communications by employing quarter-wavelength monopole antennas protruding from the aircraft's surface. These antennas, with their low frequency operations ($\lambda = 10$ m at 30 MHz), usually have a large and heavy profile, which causes considerable drag, wind noise, and increased oil consumption during the flight operations [1], [2]. Thus, the aerospace industry has made efforts to integrate the antenna structure into the aircraft skin by using conformal antennas. The conformal antenna is one of the most common antenna integration technologies used to maximize the aerodynamic performance and minimize the wind noise and weight [3]. However, it requires a structural change to insert the antenna underneath the aircraft's surface, causing increased cost and difficulty in fabrication due to the structural complexity of the aircraft. In contrast, the automobile industry has made efforts to integrate the antenna onto the window surface for FM radio reception [4]–[6]. Glass-integrated antennas show better aerodynamic characteristics, allowing for improved durability, light weight, and low wind noise characteristics [7]. Furthermore, because no structural alterations are required, the glass-integrated antennas cost much less than the conformal antennas. Although there are many advantages of the glass-integrated antennas, not enough research has been conducted to apply glass-integrated antennas to military aircrafts because of their drawbacks such as low radiation gain and narrow matching bandwidth [8].

Manuscript received February 16, 2011; revised August 22, 2011; accepted October 26, 2011. Date of publication January 31, 2012; date of current version April 06, 2012. This work was supported in part by the IT R&D program of MKE/KEIT [KI002084, A Study on Mobile Communication System for Next-Generation Vehicles with Internal Antenna Array] and in part by the MKE (The Ministry of Knowledge Economy), Korea, under the ITRC (Information Technology Research Center) support program supervised by the NIPA (National IT Industry Promotion Agency) (NIPA-2011-C1090-1121-0005).

G. Byun is with the School of Electronic and Electrical Engineering, Hongik University, Seoul, Korea.

C. Seo is with the School of Electronic Engineering, Soongsil University, Seoul, Korea.

B.-J. Jang is with the Department of Electrical Engineering, Kookmin University, Seoul 136-702, Korea.

H. Choo is with the School of Electronic and Electrical Engineering, Hongik University, Seoul, Korea (e-mail: hschoo@hongik.ac.kr).

Digital Object Identifier 10.1109/TAP.2012.2186234

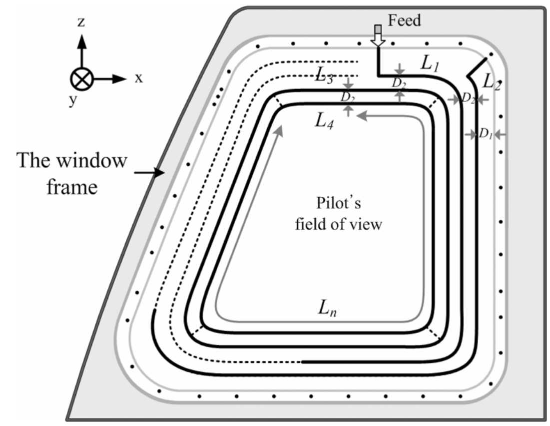

Fig. 1. Proposed antenna structure.

In this communication, we propose a glass-integrated antenna that can achieve a broader matching bandwidth and higher radiation gain compared to other electrically small antennas using two radiators with an inductively coupled feed structure. The two radiators consist of a shorted strip and a parasitic loop strip, which is employed to achieve dual-resonance. They are connected electromagnetically with the feed strip, and the coupling strength is adjusted by the distance between the radiators and the feed structure. In addition, antenna strips are designed to be placed at the outer perimeter of the window for a superior field of view by imitating the shape of the window frame. To improve the antenna's matching bandwidth and radiation gain, detailed parameters are optimized by using the genetic algorithm (GA) in conjunction with the FEKO EM simulator [9], [10]. The optimized antenna is built and installed on the left-side window of a 1/10-sized Korean Utility Helicopter (KUH-Surion) mock-up and antenna performances such as a reflection coefficient and radiation gain are measured in the 10-times higher frequency band of the military FM band (30 MHz–88 MHz). In addition, the minimum received power level of a transmitted signal from a base station is simulated according to a flight scenario to evaluate the antenna performance in a real situation. The results prove that the proposed antenna is suitable to use as a replacement for the quarter-wavelength monopole antennas for military FM radio communications.

II. Antenna Structure and Optimization

Fig. 1 shows the proposed glass antenna structure having two radiators integrated into the left-side window of the KUH-Surion. The proposed antenna has an inductively coupled feed structure which is a well-known technology providing broad matching characteristics compared to the direct feed structure [11]. The two radiators are linked electromagnetically with the feed strip and the coupling strength is controlled by the distance between the strips (D_2) and the feed strip length (L_1). The radiation gain is improved by achieving dual-resonance using two radiators consisting of a shorted strip and a parasitic loop strip. The shorted strip is grounded at the top right corner of the window frame and the length (L_2) is designed to be approximately $\lambda/4$ at the center frequency (1.25 m at 60 MHz). The total length of the parasitic loop strip (L_3, L_4) is designed to be approximately $\lambda/2$ at a lower frequency by connecting the loop strips selectively at the four corners. Antenna strips mimic the shape of the window frame so as to be fit at the outer perimeter of the window, which allows the pilot's field of view (FOV) to be located at the center of the antenna structure.

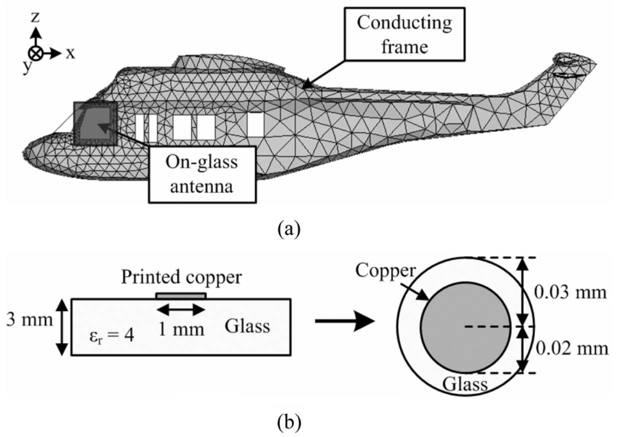

Fig. 2. EM simulation condition. (a) Geometry of the KUH-Surion, (b) coated wire method.

It enables the antenna to attain high transparency and to maximize the pilot's FOV.

Fig. 2(a) shows the geometry of the KUH-Surion with the proposed antenna located at the left-side window of the cockpit. We included almost the entire geometry in our EM simulation for an accurate estimation of antenna performance but eliminated some parts, such as propellers and the landing gears, which did not affect the antenna performance in order to reduce the simulation time. Furthermore, we added the interior components, such as floors and partitions, since the internal resonance of the aircraft also strongly affects antenna performance. To further reduce the simulation time while maintaining simulation accuracy, we applied rougher mesh triangles to the geometries where current distributions appeared relatively weak compared to other parts. As a result, the entire geometry was re-modeled to 3 300 piecewise mesh triangles, and less than two-minute simulation time was achieved for each frequency point. To estimate the antenna performance of the printed strips ($\mathrm{Width} = 1$ mm, $\sigma = 5.8 \times 10^7$) on a glass material ($\mathrm{Thickness} = 3$ mm, $\varepsilon_r = 4$), we applied a coated wire method having a radius of 0.02 mm for the inner conducting wire, and a radius of 0.03 mm for the outer coated material ($\varepsilon_r = 4$), as shown in Fig. 2(b). The proposed antenna structure was optimized by the GA in conjunction with the FEKO EM simulator and cost functions were defined as (1), (2), and (3)

$$\mathrm{Cost\ 1} = 1 - \frac{\mathrm{BW_{ANT}}}{\mathrm{BW_{FM}}} \tag{1}$$

$$\mathrm{Cost\ 2} = \frac{1}{M}\sum_{i=1}^{M} |S_{11}| \tag{2}$$

$$\text{if FOV} = 1 - \frac{S_{\mathrm{ANT}}}{S_{\mathrm{WIN}}} < 0.6, \quad \text{exclude the design.}$$
$$30\ \mathrm{MHz} \leq \text{frequency} \leq 88\ \mathrm{MHz}. \tag{3}$$

Equation (1), defined to broaden a half-power matching bandwidth, is determined by the ratio of the antenna's bandwidth $(\mathrm{BW_{ANT}})$ to the military FM radio band ($\mathrm{BW_{FM}}$, 30 MHz–88 MHz). Equation (2) shows an average reflection coefficient over M frequency points, and we used it to estimate how accurately the antenna matches to a 50 ohm system. We excluded the design having less than 60% of the pilot's FOV to ensure the maximum visual area in the window, which was considered by the ratio of the antenna area (S_{ANT}) to the entire window area (S_{WIN}, 0.56 m^2) as shown in (3).

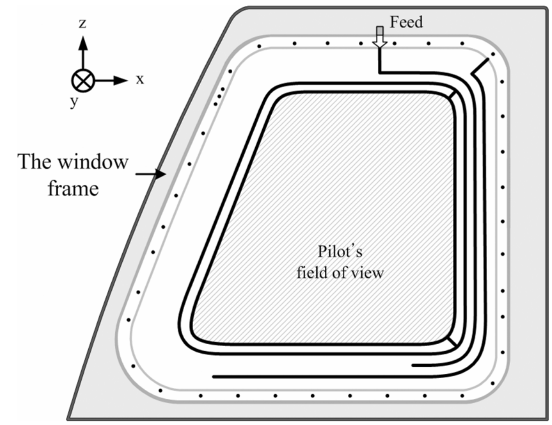

Fig. 3. Optimized antenna structure.

TABLE I
PARAMETERS OF THE OPTIMIZED ANTENNA

Parameter	Length
L_1	683 mm
L_2	821 mm
L_3	1972 mm
L_4	1823 mm
D_1	30 mm
D_2	30 mm

Fig. 3 shows the optimized antenna structure, and the detailed optimum parameters are shown in Table I. The pilot's FOV, specified in the same figure, is 63% (0.35 m^2), and the antenna strips are located at the outer perimeter of the window. Therefore, the optimized antenna has an added benefit of a superior FOV compared with other types of glass antennas.

III. Measurement and Analysis

A. Experimental Results

To verify the antenna performance, we made a 1/10-sized KUH-Surion mock-up having fourteen windows and the detailed inner structures such as partitions and floors. In our mock-up, the material of polyarcrylate that has a similar electrical property ($\varepsilon_{\mathrm{r}} = 3.5$) to a real aircraft window, was used for the downscaled window material, and a conducting sheet was pasted on the inner surface of the mock-up to provide an electrical grounding. Measurements were conducted in the 300 MHz–880 MHz band since the downscaled antenna showed the same characteristics in the 10-times higher frequency band of the original frequency. The glass-integrated antenna was installed in the mock-up, and the antenna performances, such as the reflection coefficient and radiation patterns, were measured using a horn antenna (aperture of 60 cm $\times$ 20 cm) and a network analyzer HP 8753D in a semi-anechoic chamber. To carefully filter out the reflected wave from other surrounding objects, we used a time-gating function of the network analyzer (time window of 6 ns–31 ns with the interval of 3 m). Fig. 4 shows the measured and simulated reflection coefficients of the optimized antenna. measured result shows a half-power matching bandwidth of 28% ($|\Gamma| < 3$ dB, 45 MHz–62 MHz), which agrees well with the simulated result. Fig. 5 represents the radiation gain in two directions over the frequency range, which shows a good agreement with each other. The antenna maintains the minimum radiation gain of more than -10 dBi

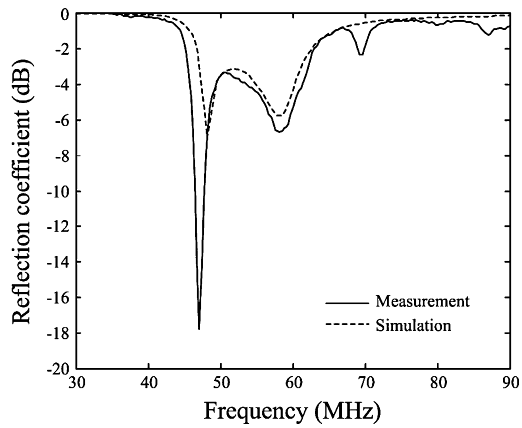

Fig. 4. Reflection coefficient of the optimized antenna.

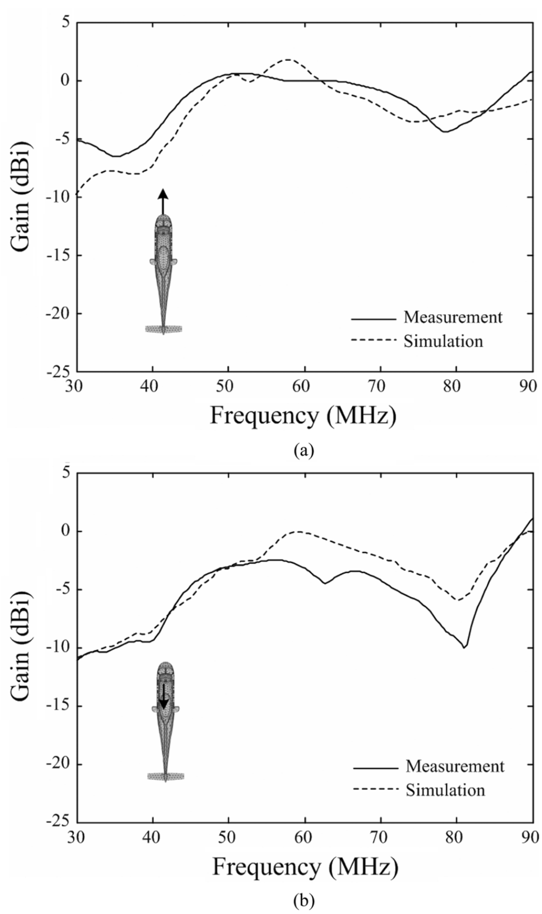

Fig. 5. Gain of the optimized antenna. (a) Front side gain, (b) back side gain.

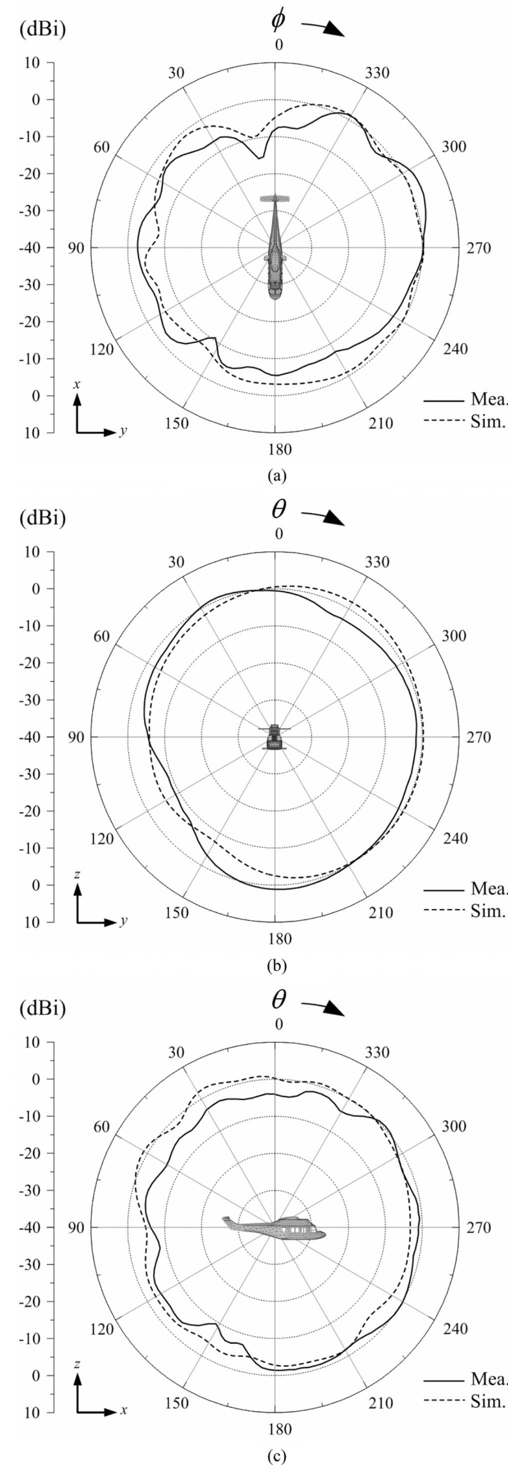

Fig. 6. Radiation patterns of the optimized antenna. (a) xy-plane (azimuth pattern). (b) yz-plane. (c) xz-plane.

in the entire military FM band, with average gains of -1.97 dBi and -5.41 dBi in the front and rear directions, respectively.

Fig. 6(a) shows an azimuth radiation pattern in *xy*-plane at 60 MHz. It reveals a good omni-directional property with a gain deviation of less than 11 dB, and the maximum gain occurs at the left side of the aircraft where the antenna is mounted. Fig. 6(b) and (c) are the radiation patterns in yz-plane and xz-plane, respectively. They also show low gain deviations of less than 10 dB; however, slight distortions appear in some directions due to the wave blockage caused by the conducting frame.

B. Operating Principles

To analyze the operating principles of the antenna and to demonstrate its broad matching characteristics from the circuit point of view, we developed a circuit model having the same impedance response. Fig. 7(a) shows the equivalent circuit model, which consists of three resonant circuits representing the feed strip, the shorted strip, and the parasitic loop strip. The feed strip and the shorted strip make resonances at 60 MHz and 48 MHz, respectively, and the parasitic loop strip connects

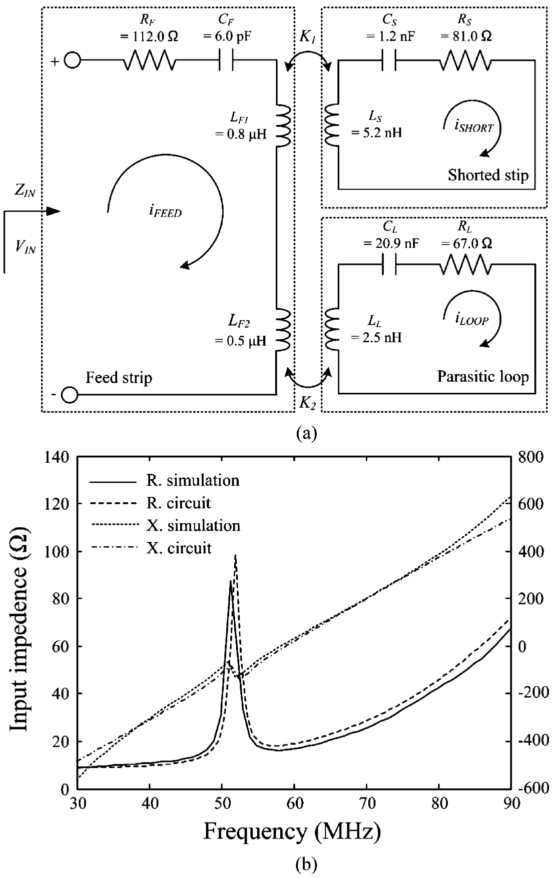

Fig. 7. Equivalent circuit model. (a) RLC circuit model, (b) input impedance.

two resonances using mutual coupling at around 50 MHz. Each circuit is inductively linked with coupling coefficients of K_1 and K_2, and the values for the lumped elements are shown in the same figure. The input impedance of the circuit model is shown in Fig. 7(b) and is compared to the EM simulation, both of which agree well with each other. The real and imaginary impedance values are separately indicated on both sides of the figure; the real part values are on the left, and the other one is shown on the right. The currents induced in the two radiators ($i_{\rm SHORT}$ and $i_{\rm LOOP}$) are determined by the coupling strength in relation to the feed current ($i_{\rm FEED}$). To verify the effect of the coupling strength, we observed the coupling coefficients by varying the distance (D_2) between the feed strip and each radiator. Then, K_1 and K_2 of the circuit were computed by solving mesh equations from Kirchhoff's voltage law (KVL), as shown in (4), (5), and (6), in the frequency domain [12]

$$V_F = \left[R_F + jw(L_{F1}+L_{F2}) + \frac{1}{jwC_F}\right] i_{\rm FEED} - jwM_1 i_{\rm SHORT} - jwM_2 i_{\rm LOOP} \quad (4)$$

$$0 = \left[R_S + jwL_S + \frac{1}{jwC_S}\right] i_{\rm SHORT} - jwM_1 i_{\rm FEED} \quad (5)$$

$$0 = \left[R_L + jwL_L + \frac{1}{jwC_L}\right] i_{\rm LOOP} - j\,wM_2 i_{\rm FEED}. \quad (6)$$

Two unknowns (M_1 and M_2) represent mutual inductances, which are proportional to the coupling coefficient, as shown in (7) and (8)

$$K_1 = \frac{M_1}{\sqrt{L_{F1}L_S}} \quad (7)$$

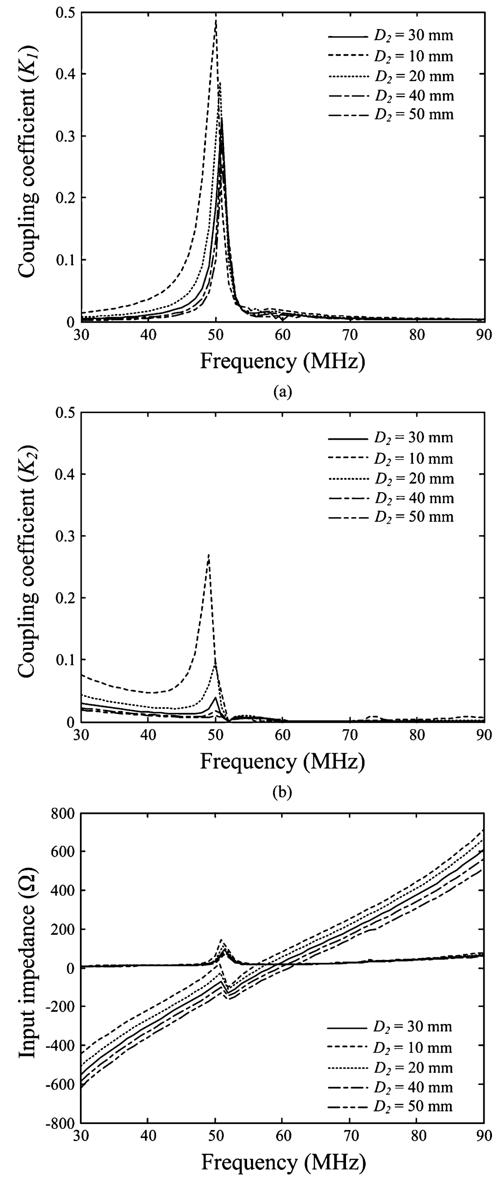

Fig. 8. Comparison of different D_2. (a) Coupling coefficient K_1, (b) coupling coefficient K_2, (c) input impedance.

$$K_2 = \frac{M_2}{\sqrt{L_{F2}L_L}}. \quad (8)$$

Fig. 8(a) and (b) show the simulated K_1 and K_2 in relation to D_2. When D_2 is denoted as 30 mm, then it shows strong coupling of K_1 and K_2 at around 50 MHz, with a peak value of 0.32 and 0.05, respectively. This means the shorted strip is more tightly coupled with the feed strip compared to the parasitic loop strip. In addition, the peak value of K_1 and K_2 decreases and shifts toward higher frequency as D_2 increases. Fig. 8(c) shows the input impedance in relation to D_2. As expected, the matching characteristic was highly dependent on the coupling strength, and thus, the optimum distance D_2 can be found for the broadband impedance matching.

To examine the antenna more closely from the EM field standpoint, we observed the H-field distributions at 60 MHz, as shown in Fig. 9. The inset of the figure indicates the cross section where the H-field was observed, and the dotted circles indicate the positions of antenna strips at the cross section. The positions of two parasitic loop strips and the

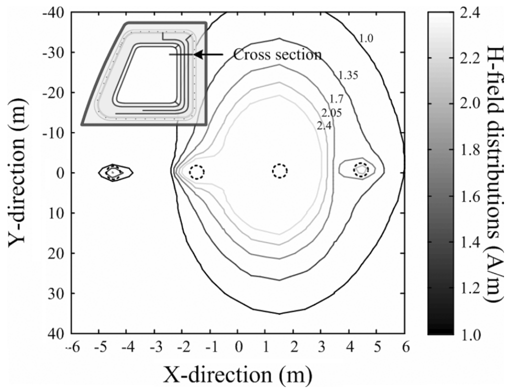

Fig. 9. H-field distributions.

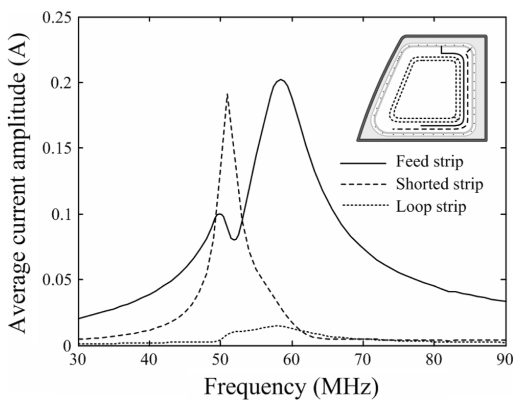

Fig. 10. Current distributions.

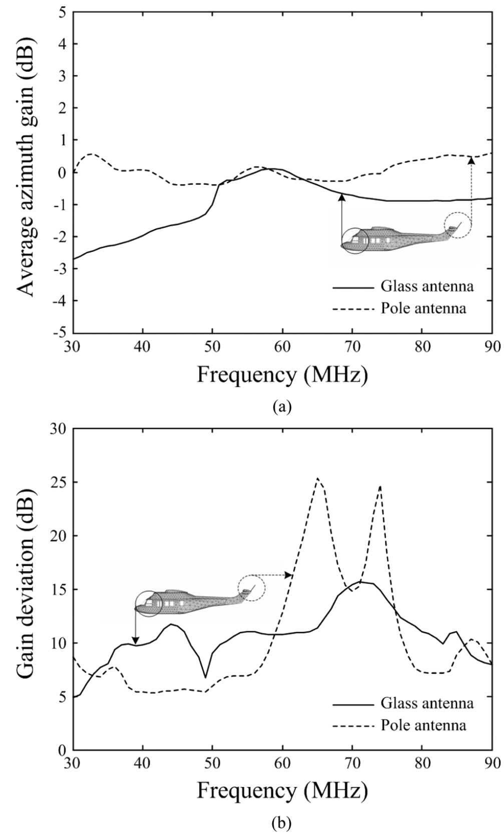

Fig. 11. Comparison with a quarter-wavelength monopole antenna. (a) Average azimuth gain, (b) gain deviation.

feed strip are shown from the left, and the shorted strip is marked with the far-right circle. Stronger H-field distributions were observed at the feed strip and the shorted strip compared to the loop strip, and this result agreed to the ratio between K_1 and K_2. In Fig. 10, we plotted the average current amplitude at each strip over the frequency range. As in the H-field distributions, the shorted strip shows higher current amplitude compared to the loop strip at 50 MHz, and this, consequently, verifies that the mutual coupling between the feed and each radiator determines the important antenna characteristics, such as current distributions and near field distributions.

C. Evaluations

To evaluate the antenna performance, we compared the optimized antenna with a quarter-wavelength monopole antenna that is commonly used for military FM radio communications. As shown in Fig. 11(a) and (b), we calculated the azimuth gain and gain deviation that are especially important for aircraft applications, since the most incoming signals come from the horizontal direction [13]. The average gain of the proposed antenna is -2.7 dBi at the lowest frequency of 30 MHz, which is only 2.7 dB lower than that of a conventional quarter-wavelength monopole having a resonance at 60 MHz. This gain characteristic may satisfy engineering needs if the antenna is accompanied by proper amplifiers. In addition, contrary to the fact that our antenna's deviation does not exceed 15 dB in the entire military FM band, the quarter-wavelength monopole antenna shows a peak deviation value of around 25 dB, which is caused by the pattern's null point (at $\theta = 90^\circ, \varphi = 0^\circ, -22$ dBi). This result possibly causes unexpected disruption in communication between the aircraft and the base station.

IV. Conclusion

We have investigated the design of a glass-integrated antenna using a coupled feed structure that has a high radiation gain and broad matching characteristics for aircraft applications. The proposed antenna consists of a feed strip and two radiators, and the antenna strips imitate the shape of the window frame to ensure the pilot's FOV as unobstructed as possible. We placed the feed strip between the two radiators to connect electromagnetically in relation to the feed current. The coupling strength was controlled by varying the distance between strips, and the detailed parameters were optimized by using the GA in conjunction with the FEKO EM simulator. The optimized antenna was built and installed on a 1/10-sized mock-up and antenna performance, such as reflection coefficient and radiation patterns, was measured in a semi-anechoic chamber. The measurement was conducted in the frequency band of 300 MHz–880 MHz, since the antenna showed the same characteristics in the 10-times higher frequency band. The antenna showed a half-power matching bandwidth of 28% and an average bore-sight gain of -2.50 dBi in the military FM band. We then analyzed the operating principles using the equivalent circuit model and field distributions. The results demonstrate the antenna's suitability for use in aircraft applications.

References

[1] L. Low, R. Langley, R. Breden, and P. Callaghan, "Hidden automotive antenna performance and simulation," *IEEE Trans. Antennas Propag.*, vol. 54, no. 12, pp. 3707–3712, Dec. 2006.

[2] C. Shimizu and Y. Kuwahara, "Analysis of a diversity antenna mounted on the vehicle for FM radio," in *Proc. IEEE Int. Symp. Antenna Propag.*, Honolulu, HI, Jun. 2007, vol. 1, pp. 1068–1071.

[3] L. Josefsson and P. Persson, *Conformal Array Antenna Theory and Design*. New York: Wiley, 2006.

[4] R. Abou-Jaoude and E. K. Walton, "Numerical modeling of on-glass conformal automobile antennas," *IEEE Trans. Antennas Propag.*, vol. 46, no. 6, pp. 845–852, Jun. 1998.

[5] W. Kang and H. Choo, "Design of vertical lines for vehicle rear window antennas," *Microw. Opt. Technol. Lett.*, vol. 52, no. 6, pp. 1445–1449, Jun. 2010.

[6] Y. Noh, Y. Kim, and H. Ling, "Broadband on-glass antenna with mesh-grid structure for automobiles," *Electron. Lett.*, vol. 41, no. 21, pp. 1148–1149, Oct. 2005.

[7] S. Ahn and H. Choo, "A systematic design method of on-glass antennas using mesh-grid structures," *IEEE Trans. Veh. Technol.*, vol. 59, no. 7, pp. 3286–3293, 2010.

[8] L. B. Felsen and N. Marcuvitz, *Radiation and Scattering of Waves*, 2nd ed. New York: IEEE Press, 1994.

[9] Y. Rahmat-Samii and E. Michielssen, *Electromagnetic Optimization by Genetic Algorithms*. New York: Wiley, 1999.

[10] EM Software & Systems, FEKO Suite 5.5 [Online]. Available: http://www.feko.info

[11] D. M. Pozar, "Input impedance and mutual coupling of rectangular microstrip antennas,," *IEEE Trans. Antennas Propag.*, vol. AP-30, pp. 1191–1196, Nov. 1982.

[12] C. K. Alexander and M. N. O. Sadiku, *Fundamentals of Electric Circuits*, 2nd ed. New York: McGraw-Hill, 2004.

[13] A. S. Bajwa and J. D. Parsons, "Small-area characterization of UHF urban and suburban mobile radio propagation," *Proc. Inst. Elec. Eng.*, vol. 129, no. 2, pp. 102–109, Apr. 1982.

[14] C. A. Balanis, *Antenna Theory: Analysis and Design*, 3rd ed. New York: Wiley, 2005.

[15] M. E. Van Valkenburg, *Reference Data for Engineers: Radio, Electronics, Computer and Communications*, 9th ed. Oxford, U.K.: Newnes, 2001.

Biconical Antenna Over Ground Plane

James L. McDonald and Dejan S. Filipovic

***Abstract*—A bicone over a finite ground plane is designed that has on average 2.8 dB more gain over a 10:1 band than its free-space counterpart. Metrics are established that enable a better understanding of antenna performance taking into account both the impedance and the radiation pattern. The effects of a finite sized ground plane are explored. To improve antenna performance over electrically small ground plane, a recessed geometry is proposed and studied. A recessed ground plane and bicone configurations are found that have better performance than the free-space bicone over 70% of the 10:1 band. Theoretical results are well supported by the measurements.**

***Index Terms*—Antenna radiation patterns, broadband antennas, conical antennas, dipole antennas, impedance matching.**

I. Introduction

When a bicone [1] is placed above the ground plane, its performance will differ from that in free-space. In [2] the effect of infinite ground plane on antenna factor is studied for the purpose of radiated emission testing. It is seen that the effect is more pronounced on a horizontally polarized bicone due to the stronger coupling to its image. However, this study was specific to the application and the fundamental understanding off, and impact on the performance parameters of interest for other applications (communications, electronic warfare, etc.) are difficult to assess. Finite size ground plane effects on asymmetrical bicone and classical monocone are studied in [3] and [4], respectively. In the former, the beam tilt is contributed to the bicone structure itself, rather than to the combined effect with the close ground plane. In [5], the lower cone of a bicone is directly integrated with a designed finite size circular ground plane to reduce the turn-on frequency by about 40%. A corrugated ground plane is proposed in [6] to improve the performance of a conical monopole and obtain better stability of radiation patterns. Finally, a theoretical metamaterial construct within the transformational electromagnetic analysis is used in [7] to recover classical monopole performance from a resonant monopole embedded in a deep ground plane recess. This approach is interesting, however only a narrowband effect is shown and the practical implementation has yet to be demonstrated.

Manuscript received November 23, 2010; revised August 08, 2011; accepted October 26, 2011. Date of publication January 31, 2012; date of current version April 06, 2012. This work was supported by FIRST RF Corp., Boulder, CO 80301 USA.

J. L. McDonald is with FIRST RF Corp., Boulder, CO 80301 USA (e-mail: jlmcd76@gmail.com).

D. S. Filipovic is with the Department of Electrical, Computer and Energy Engineering, University of Colorado, Boulder, CO 80309 USA (e-mail: dejan@colorado.edu).

Digital Object Identifier 10.1109/TAP.2012.2186228

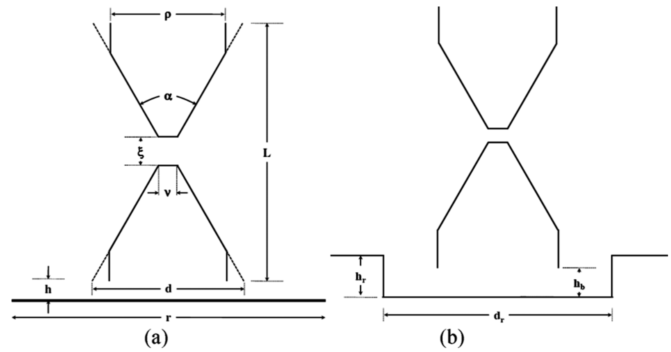

Fig. 1. The structural parameters of a modified bicone over a ground plane (a), and its recess (b).

In this letter, we evaluate the impedance, beam efficiency, and minimum gain within application driven field of view of wideband bicones over infinite and finite size ground planes and introduce a small recess in the ground plane for further improvements. Specifically, the optimal 2 dBi monocone geometry from our earlier work ($\alpha = 80^\circ, \rho/d = 52\%$) [8] is used as a baseline for the antenna geometry. In [8] the monocone was optimized for its maximal bandwidth with minimum realized gain of 2 dBi inside a 39° field of view. This monocone geometry is converted to that of a bicone followed by the optimization of the feed region parameters for impedance match and pattern stability. It is found that the optimal feed dimensions are $\nu = \lambda_0/69$, and $\xi = \lambda_0/300$, where λ_0 is the wavelength of the lowest frequency modeled, 2 GHz. This bicone is placed over a ground plane, as shown in Fig. 1(a), and it is studied here as an alternate geometry to a monocone and free-space bicone. By exploring coupling effects generated when the bicone is placed near a ground plane, its low-frequency resistance is increased, allowing a reduction in electrical height of the antenna. The effects of the separation from the ground plane are examined and contrasted with a free-space bicone.

II. Performance Metrics

For evaluation of the antenna performance three performance metrics are used. To characterize impedance match the optimized characteristic impedance, $R_{\rm opt}$, is chosen such that the reflection coefficient over the desired bandwidth is minimized. This value is computed using